AIP | Journal of Applied Physics

On the role of disorder on graphene and graphene nanoribbon-based vertical tunneling transistors

Nayereh Ghobadi and Mahdi Pourfath

Citation: Journal of Applied Physics **116**, 184506 (2014); doi: 10.1063/1.4901584
View online: http://dx.doi.org/10.1063/1.4901584
View Table of Contents: http://scitation.aip.org/content/aip/journal/jap/116/18?ver=pdfcov
Published by the AIP Publishing

On the role of disorder on graphene and graphene nanoribbon-based vertical tunneling transistors

Nayereh Ghobadi[1] and Mahdi Pourfath[1,2,a)]
[1]*School of Electrical and Computer Engineering, University of Tehran, P.O. Box 14395-515, Tehran, Iran*
[2]*Institute for Microelectronics, TU Wien, Gusshausstrasse 27–29/E360, 1040 Vienna, Austria*

(Received 6 September 2014; accepted 1 November 2014; published online 13 November 2014)

In this work, the characteristics of vertical tunneling field-effect transistors based on graphene (VTGFET) and graphene nanoribbon heterostructure (VTGNRFET) in the presence of disorder are theoretically investigated. An statistical analysis based on an atomistic tight-binding model for the electronic bandstructure along with the non-equilibrium Green's function formalism are employed. We study the dependence of the averaged density of states, transmission probability, on- and off-state conductances, on/off conductance ratio, and transfer characteristics on the substrate induced potential fluctuations and vacancies. In addition, the variabilities of the device characteristics due to the presence of disorder are evaluated. It can be inferred from the results that while introducing vacancies cause a relatively modest suppression of the transmission probability, potential fluctuations lead to the significant increase of transmission probability and conductance of the device. Moreover, the results show that the transport properties of VTGFET are more robust against disorder compared to VTGNRFET. © *2014 AIP Publishing LLC*. [http://dx.doi.org/10.1063/1.4901584]

I. INTRODUCTION

Graphene-based nanoelectronic devices have attracted a tremendous research interest due to the excellent electronic, optical, and mechanical properties.[1] The absence of an energy bandgap, however, results in high off-state leakage current and a relatively low on/off current ratio, which in turn limits the application of graphene FETs (GFETs) for digital applications. The limitations of conventional GFETs have motivated researchers to focus on new structures such as graphene-based heterostructures.[2,3] Recently, a graphene tunneling FET based on a vertical graphene heterostructure (VTGFETs) has been proposed.[4] The source and drain contacts of this structure are made of a monolayer of graphene and the tunneling barrier is composed of hBN or MoS_2.[4] VTGFETs exhibit room-temperature switching ratios of ≈50 and ≈10 000 for hBN and MoS_2, respectively.[4] The operation of this device is based on the voltage tunability of the density of states (DOS) in graphene and of the effective height of the tunneling barrier.[4] Using armchair GNRs instead of graphene as the base material for the source and drain contacts (VTGNRFETs) leads to a significantly larger on/off current ratio due to the presence of an energy gap in GNRs.[5]

In order to properly evaluate the applicability and assess the performance of VTGFETs and VTGNRFETs, the effects of non-idealities should be investigated. Such effects have been extensively studied for conventional GFETs and GNRFETs.[6–8] Such analysis, however, is missing for VTGFETs and VTGNRFETs. In this paper, we present a comprehensive study of the influence of various sources of disorder on the characteristics of VTGFETs and VTGNRFETs. We employ an atomistic tight-binding model along with the non-equilibrium Green's function (NEGF) formalism over an ensemble of many statistically generated devices.

The paper is organized as follows: after a brief introduction in Sec. I, the device structure and the operational principle are briefly explained in Sec. II. In Sec. III, the models and numerical methods are described. The roles of substrate charged impurities and vacancies on the characteristics of VTGFET and VTGNRFET are discussed in Sec. IV and concluding remarks are presented in Sec. V.

II. DEVICE OPERATION PRINCIPLE

The sketch of a VTGFET/VTGNRFET is shown in Fig. 1(a) where the source and drain contacts are assumed to be monolayers of graphene/GNR. A few layers of hBN ($N = 2 - 6$) serve as the tunneling barrier between the source and drain contacts. A 300 nm layer of SiO_2, that corresponds to experimental structure in Ref. 4, is used as the gate oxide. The applied gate voltage, V_G, controls the tunneling current between source and drain by modulating the tunneling barrier height and carrier concentration. A positive gate-source voltage increases the concentration of electrons and results in n-type operation corresponding to off-state, see Fig. 1(c), whereas a negative gate-source voltage leads to p-type device operation and switches on the device, see Fig. 1(d). The drain-source bias voltage, V_B, gives rise to the tunneling current through the hBN layers. In VTGFET with ideal graphene and hBN sheets, the valence and conduction band edges of hBN are at energies of −1.4 eV and 3.34 eV, respectively [see Fig. 1(b)]. The current of carriers with energies between −1.4 eV and 3.34 eV is due to tunneling and thermionic otherwise. As shown in Fig. 1(e), a similar operation principle holds for VTGNRFETs except a parabolic dispersion relation and the presence of an energy gap, which leads to a smaller off-current.

a)Electronic mails: pourfath@ut.ac.ir, pourfath@iue.tuwien.ac.at

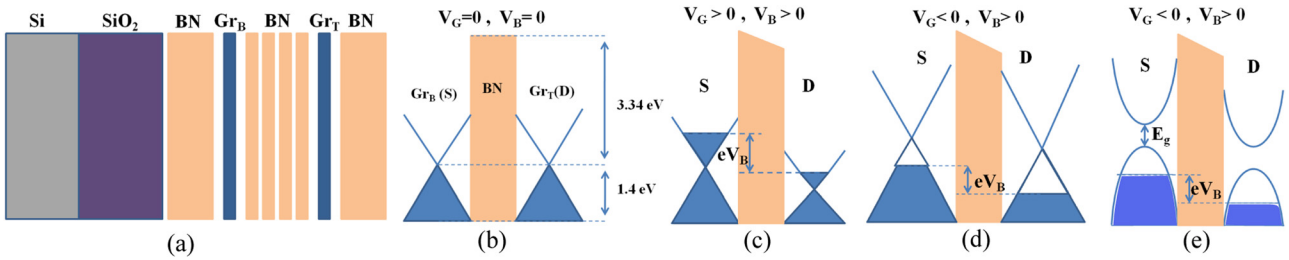

FIG. 1. (a) The sketch of VTGFET and VTGNRFET. The band structure and operation principle for a VTGFET under (b) flat band condition, (c) off-state, and (d) on-state. (e) The band structure of a VTGNRFET in the on-state. The source and drain are denoted by S and D, respectively.

III. MODELS AND METHODS

A. Tight-binding model and transport equations

An atomistic tight-binding model (Table I) along with the NEGF formalism[11] are employed for a quantum mechanical description of carrier transport in VTGFET and VTGNRFET. As shown in Fig. 2(a), a two-electrode structure is assumed for improved electrical characteristics.[5] All hBN layers are arranged in the Bernal (AB) stacking.

To study VTGFETs, where the source and drain graphene sheets are infinitely extended along the transverse direction, a periodic boundary condition can be imposed.[5,13] Implementation of periodic boundary conditions using k-space formalism, however, does not allow to model graphene sheets with disorders. To circumvent this problem, one can treat the edges as virtual contacts with appropriate self-energy matrices.[12] For this purpose, the structure shown in Fig. 2(b) can be used. In this structure, a single monolithic virtual contact surrounds the central device region. This open-boundary condition can be modeled by a self-energy (Σ_{inf}) that can be obtained from the boundary-free real-space Green's function of a graphene sheet without disorder.[12] To find the boundary-free real-space Green's function, one should first evaluate the Green's function in k-space corresponding to the infinitely extended system.[5] The retarded Green's function of the device with four contacts reads as

$$G_k = [(E + i\eta)I - H_{k_y} - \Sigma_{\text{S1}_{k_y}} - \Sigma_{\text{S2}_{k_y}} - \Sigma_{\text{D1}_{k_y}} - \Sigma_{\text{D2}_{k_y}}]^{-1}. \tag{1}$$

$k_y = 2n\pi/W$ represents the transverse wavevector, where n is an integer, $W = Na_0$ is the width of the device, $a_0 = \sqrt{3}a_{\text{c-c}}$ is the width of the graphene unit cell, and $a_{\text{c-c}}$ is the bonding length of carbon atoms in graphene. In this work, we used $N = 64$ and $n = [-32, 31]$. $\Sigma_{\text{S1,S2}}$ and $\Sigma_{\text{D1,D2}}$ in Eq. (1) are the self-energies of the source and drain contacts in k-space. By inverse Fourier transforming over the transverse wavevector, the real-space Green's function for the central device region is obtained as[12]

$$G_{mn} = \sum_k G_{k_y} \exp\left(-ik_y(R_m - R_n)\right)/N_m N_n, \tag{2}$$

where R_m and R_n represent the position of atoms in the central device region. The size of G is $N \times N$, where N is the number of atoms in the central region. The summation in Eq. (2) is performed on 64 equidistant grid points for the transverse wavevector k_y. Using the real space Green's function and the Hamiltonian of the central device region, the open-boundary self-energy is obtained[12]

$$\Sigma_{\text{inf}} = EI - H - G^{-1}. \tag{3}$$

Knowing the open-boundary self-energy, the Green's function can be calculated

$$G_r = [EI - H - U - \Sigma_{\text{S1}} - \Sigma_{\text{S2}} - \Sigma_{\text{D1}} - \Sigma_{\text{D2}} - \Sigma_{\text{inf}}]^{-1}. \tag{4}$$

The electrostatic potential and other sources of potential perturbation, such as charged impurities, in the central device region are included in U. Knowing the retarded Green's function, the transmission probability between the contacts j and k can be evaluated

$$T_{jk} = \text{Trace}[\Gamma_j G_r \Gamma_k G_r^{\dagger}], \tag{5}$$

where $j = \text{S}_1, \text{S}_2, k = \text{D}_1, \text{D}_2$, and $\Gamma(E) = i[\Sigma(E) - \Sigma^{\dagger}(E)]$ is the broadening function of the respective contact. Finally, the current between the contacts j and k is given by

TABLE I. Tight-binding parameters for heterostructure of graphene and hBN.[9,10] All parameters are expressed in terms of electron-volt.

C_{onsite}	B_{onsite}	N_{onsite}	t_{CC}	t_{BN}	$t_{\perp_{\text{GrBN}}}$	$t_{\perp_{\text{BNBN}}}$
0	3.34	−1.4	2.64	2.79	0.43	0.6

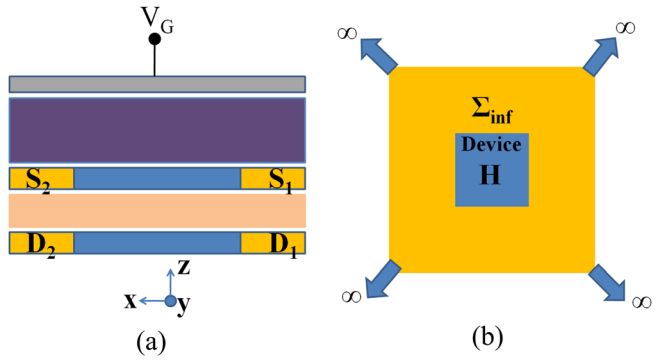

FIG. 2. (a) The sketch of the simulated structures (VTGFET and VTGNRFET), which consist of two source and drain contacts for improved electrical characteristics.[5] (b) The structure with an open-boundary condition in which the edges are treated as a single monolithic virtual contact.[12]

$$I_{jk} = \frac{2q^2}{h}\int T_{jk}(E)\big(f_j(E) - f_k(E)\big)dE\,, \tag{6}$$

where $f(E)$ is the Fermi function. The total current between the source and drain contact is $I = \sum_{j,k} I_{jk}$. In the linear response regime, the conductance of the device can be approximated by

$$G = \mathrm{G}_0 \int \left(-\frac{\partial f}{\partial E}\right) T(E)dE, \tag{7}$$

where $\mathrm{G}_0 = 2\mathrm{e}^2/\mathrm{h}$. Room temperature operation is assumed in this work. The electrostatic potential is self-consistently evaluated using the approach described in Ref. 14.

B. Disorder model

Even high quality SiO_2 substrates contain an impurity concentration of about $10^{11}\mathrm{cm}^{-2}$. Charged impurities result in potential fluctuations on the graphene/GNR sheets. In order to describe these potential fluctuations, a random Gaussian potential profile is widely used[15]

$$U(r_i) = \sum_{n=1}^{N_{\mathrm{imp}}} U_n \exp\left(-\frac{|r_i - R_n|^2}{2\xi^2}\right), \tag{8}$$

where $U(r_i)$ is the effective induced potential due to N_{imp} impurities. These impurities are centered at random lattice sites R_n, which their distance from the source graphene sheet (Z_n) is assumed to be between 0 and 2 nm. U_n is the amplitude of induced potential of each impurity, which lies between 50 meV and 150 meV.[16,17] $\xi > a_0$ is the correlation length or the potential range, which is considered between $1a_0$ and $5a_0$ ($a_0 = \sqrt{3}a_{\mathrm{c-c}} = 2.46$Å is the lattice constant). The effect of substrate charged impurity is added to the diagonal elements of the central region Hamiltonian H. Three cases for charged impurities have been considered. First, both negative and positive charged impurities are considered. Second, only positive charges and finally only negative charges are included. These three profiles are denoted by PN, P, and N labels, respectively.

The vacancies are modeled by randomly removing of carbon atoms in graphene and GNR sheets, which is denoted by VC, or boron and nitrogen atoms in hBN sheets, which is denoted by VBN. The ratio of the removed atoms to the total number of atoms in each sheet is represented by P_V. In the Hamiltonian of the device, the hopping parameters of removed atoms are set to zero.

IV. RESULTS AND DISCUSSIONS

VTGFETs are examined with 2, 4, and 6 layers of hBN and VTGNRFETs are investigated for GNR widths of 2 nm and 3.4 nm. All hBN sheets are arranged in the Bernal (AB) stacking. Assuming an interlayer distance of 3.5 Å,[9] the thickness of the hBN dielectric lies in the range of 1–2.5 nm. In addition to the geometrical parameters, the effect of disorder type and strength on the device characteristics is studied. The applied gate voltage is limited by the gate oxide breakdown, which is about 1 V/nm for SiO_2. The drain-source bias voltage is limited to about 1.4 V. For a given set of geometrical and disorder parameters, 100 samples are stochastically generated. Using Eq. (7), the conductance of each device is separately evaluated, then by performing an ensemble average over all samples the average conductance is evaluated. The on-state conductance is defined at $E_{\mathrm{F}} = -1$ eV, which is located in the hole-dominated regime, while the off-state conductance is calculated in the electron-dominated regime at $E_{\mathrm{F}} = 3$ eV. In VTGNRFETs, in addition to G_{off_1} which is evaluated at $E_{\mathrm{F}} = 3$ eV, G_{off_2} is calculated in the middle of energy bandgap, $E_{\mathrm{F}} = 0$ eV, which results in a relatively smaller off-state conductance and a larger on/off conductance ratio ($G_{\mathrm{on}}/G_{\mathrm{off}_2}$) in comparison with VTGFETs.

A. Substrate induced potential fluctuations

Fig. 3 presents the effect of potential fluctuations with PN, P, and N charges on the transmission probability and DOS of a VTGFET and a VTGNRFET with 6 layers of hBN and GNR width of 2 nm at flat band condition. Positive charged impurities decrease the tunneling barrier for holes, whereas negative ones decrease the tunneling barrier for electrons. In armchair nanoribbons, where the ground state is non-magnetic and on-site potentials are initially assumed to be zero, even in the presence of weak potential fluctuations,

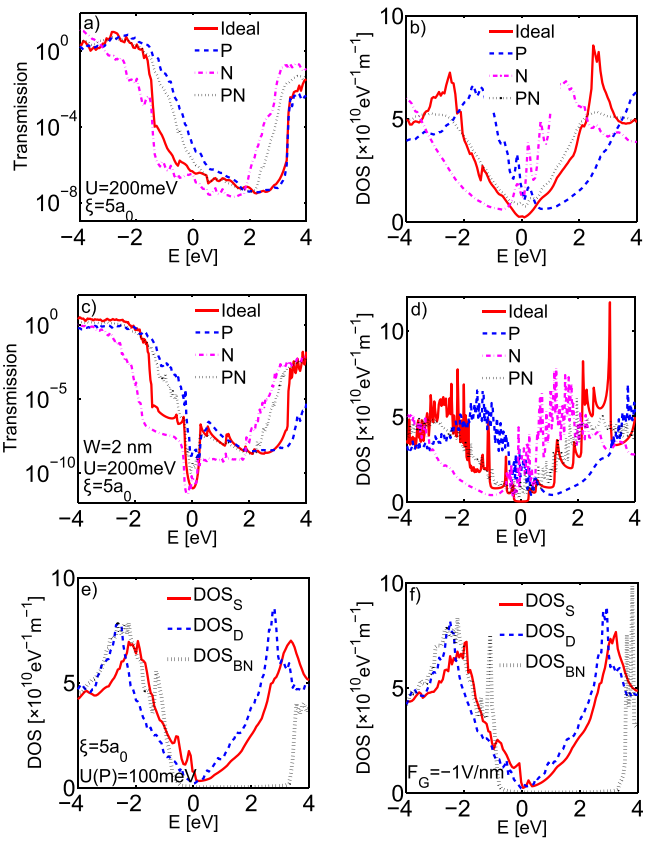

FIG. 3. The average transmission and DOS of the source graphene/GNR sheet of (a) and (b) VTGFET, and (c) and (d) VTGNRFET with 6 layers of hBN in the presence of potential fluctuations with positive (P), negative (N), and both positive and negative (PN) charges. The DOS of the source and drain graphene/GNR sheets in the presence of (e) potential fluctuations with positive charges and (f) applied gate electric field.

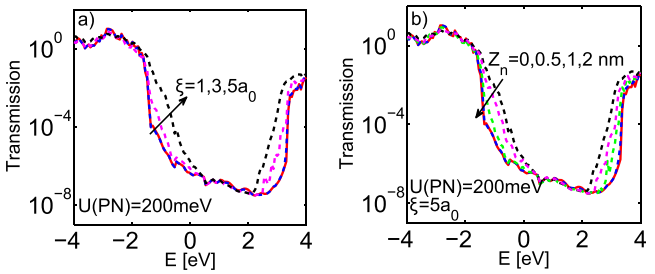

FIG. 4. The dependency of the average transmission of VTGFET on the (a) correlation length and (b) vertical position of charged impurities with PN charges.

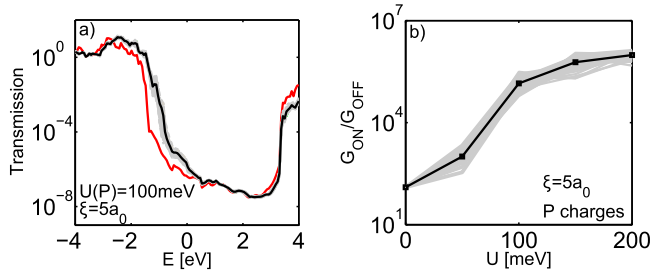

FIG. 6. (a) The average transmission probability over different samples (solid-black line) and the transmission probability of each sample (gray lines) and the transmission probability of a perfect VTGFET (solid-red line). (b) The average on/off conductance ratio over different samples and the on/off conductance ratio of each sample in the presence of potential fluctuations with positive (P) charges.

the DOS and transmission probability are significantly affected.[8,18] In a VTGNRFET, localized states with non-zero DOS exist in the bandgap which can be attributed to potential wells formed by fluctuations.[18] These states increase the off-state conductance.

It is worthwhile to note that charge trapping can occur during the operation and can influence the potential distribution and the device characteristics. This charge trapping is mostly due to positive and negative bias temperature instability (BTI), which is the most reliability concerns in the nanodevices and create both oxide as well as interface traps (ITs). BTI in VTGFETs can be understood using standard methods previously developed for Si technologies, if the degradation dynamics are expressed in terms of a Dirac point voltage shift and modulation of carrier concentration and tunneling current rather than a threshold voltage shift.[19] As shown in Figs. 3(e) and 3(f), the influence of charged impurities can be simply explained in analogy to the effect of an extra applied gate electric field, which results in the change of carrier concentration and tunneling current. The modeling of the NBTI by the use of a gate voltage source has been proposed and implemented for Si-MOSFETs.[20]

Fig. 4 shows the effect of the correlation length and the position of impurities on the transmission probability. As the correlation length is an indication of the effective potential range, the number of atoms which are affected by charged impurities increases with this parameter. Fig. 4(a) shows that as ξ increases the effective tunneling regime is reduced and the device is more affected by charged impurities. The comparison of transmission probabilities shown in Fig. 4(b) demonstrates that as Z_n decreases—corresponding to impurities being located closer to the graphene or GNR's plane—the device is more influenced by charged impurities.

Fig. 5 presents the on-, off-state conductances, and on/off conductance ratio of a VTGFET and a VTGNRFETs as a function of the potential fluctuation strength. In the presence of P charges, because of the decrease of the hole tunneling barrier, the weight function $\partial f/\partial E$ in Eq. (7) encompasses the thermionic regime transmission [cf. transmission curves around $E=-1$ eV in Figs. 3(a) and 3(c)]. Therefore, the on-state conductance significantly increases with disorder strength and the off-state conductance, which is dominated by the electron tunneling, is slightly reduced due to moderate variation of the electron tunneling barrier. On the other hand, an increase of N charges decreases the on-state conductance and enhances the off-state conductance. For larger values of negative charged impurities, the polarity of the device is reversed, see Figs. 5(c) and 5(f). The influence of PN charges can be explained as the superposition of P and N charges. The off-state conductance of VTGNRFET, which is estimated in the middle of energy bandgap (G_{off_2}), increases with P and PN charges. This behavior is attributed to midgap states induced by charged impurities. In the case of N charge, however, due to the reduction of the transmission in the hole tunneling region G_{off_2} varies smoothly.

The transmission probability and on/off conductance ratio for many samples and the average transmission probability and on/off conductance ratio of a VTGFET in the presence of potential fluctuations with positive (P) charges are shown in Fig. 6. The standard deviations of the on/off conductance ratio as a percentage of the average value in the presence of P charges are 29.2% and 15.1% for a VTGFET and VTGNRFET with a width of 2 nm, respectively.

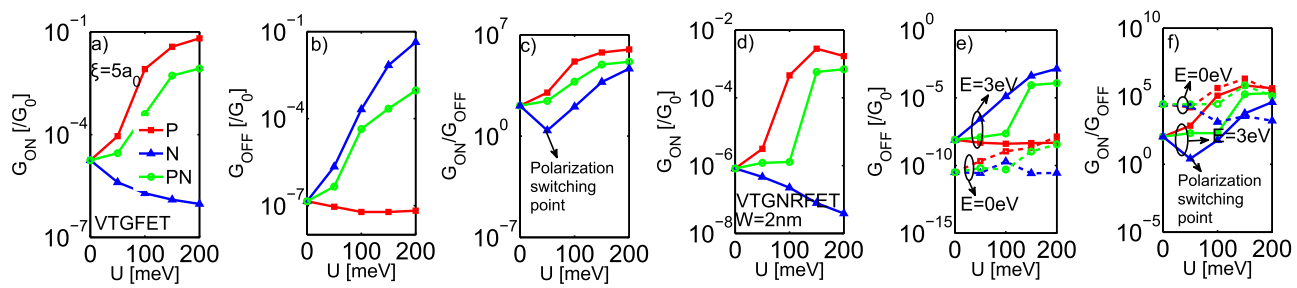

FIG. 5. The dependency of the on-, off-state conductances, and on/off conductance ratio on the amplitude of potential fluctuations with P, N, and PN charges. (a)-(c) VTGFET and (d)-(f) VTGNRFET with 6 layers of hBN.

TABLE II. The relative change in the on- and off-state conductances of VTGFETs at various numbers of hBN layers in the presence of substrate charged impurity. $U = 200\,\text{meV}$ and $\xi = 5a_0$.

No. of hBN layers	$\Delta G_{on}/G_{on}(P)$	$\Delta G_{on}/G_{on}(PN)$	$\Delta G_{off}/G_{off}(N)$	$\Delta G_{off}/G_{off}(PN)$
2	73	12	29	4
4	1.4×10^3	130	1.3×10^4	1.2×10^3
6	3.6×10^3	474	3.1×10^5	6.6×10^3

The relative change[21] in the on- and off-state conductances of VTGFET at various numbers of hBN layers in the presence of charged impurities is listed in Table II. Devices with thicker hBN dielectric are more influenced by potential fluctuation and exhibit larger relative changes in the conductance. As the thickness of hBN dielectric increases, the charged impurity induced potential difference between the source and drain graphene/GNR sheets increases. For a better comparison, Fig. 7 compares the transfer characteristics of VTGFET and VTGNRFET with a width of 2 nm in the presence of P, N, and PN charges. The increase of the tunneling current by P and PN charges is related to the reduction of the hole tunneling barrier and also the formation of mid-gap states [see Fig. 3(c)].

B. Vacancy

Figs. 8 and 9 indicate the averaged DOS and transmission probability of VTGFET and VTGNRFET, respectively, with 6 layers of hBN at various percentage of vacancies of carbon atoms (VC) and vacancies of boron and nitrogen atoms (VBN). By introducing vacancies in a graphene sheet, non-dispersing (flat) bands appear near the Fermi level. These bands arise from the localization of charges and dangling bonds around the vacant sites.[22,23] Furthermore, in the presence of vacancies, the crossing of the valence and conduction bands at the K-point and the electron-hole symmetry of graphene are removed. The linearly dispersing valence and conduction bands observed in perfect graphene are shifted away from the charge neutrality point.[22,24] Therefore, in defected devices, an increase in the transmission probability in the electron-dominated regime and a decrease of that in the hole-dominated regime occurs.[22,24] On the other hand, the increase of vacancies reduces the number of available

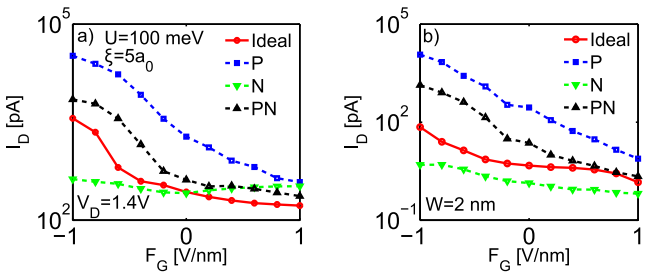

FIG. 7. Drain currents as functions of the applied gate electric field in the presence of charged impurities for (a) VTGFET and (b) VTGNRFET with 6 layers of hBN.

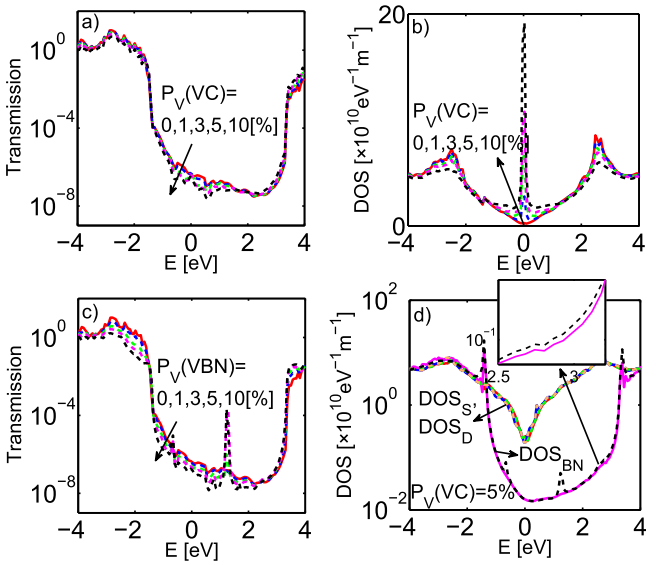

FIG. 8. The average transmission probability and DOS of a VTGFET with 6 layers of hBN at various percentage of vacancies (P_V) of carbon atoms (VC) (a) and (b) and of boron and nitrogen atoms (VBN) (c) and (d).

atomic sites and vanishing of hopping between the atomic orbitals. Therefore, as P_V increases the transmission probability of VTGFET decreases. Vacancies reduce the effective width of GNRs and result in the increase of energy bandgap, see Fig. 9(a). However, midgap states induced by vacancies increase the transmission probability within the bandgap. The small peaks of the transmission probability in the bandgap are due to hopping between localized states.[25]

During the CVD growth, vacancies can be formed in hBN sheets,[26] which in turn enhance defect-assisted tunneling.[27–29] This can be observed as the increase of the transmission coefficient at some energy points, which are in accordance with the peaks of the DOS of hBN sheets [see Figs. 8(c) and 8(d)]. In the presence of boron vacancies, the

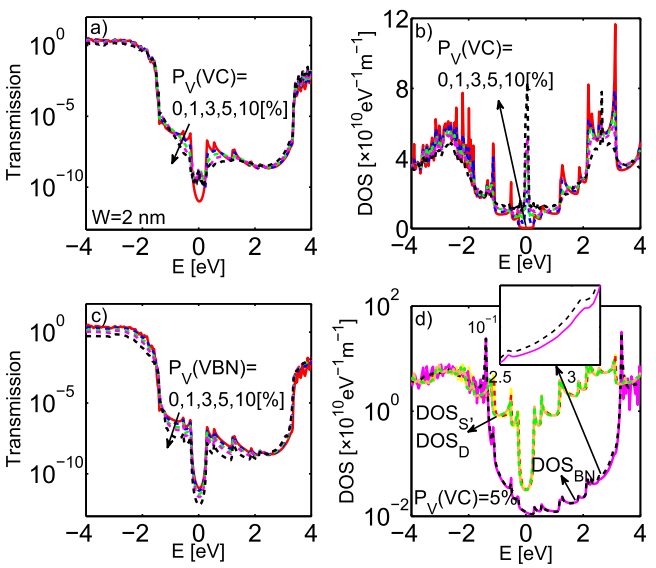

FIG. 9. The average transmission probability and DOS of a VTGNRFET with a width of 2 nm and 6 layers of hBN at various percentage of vacancies (P_V) of carbon atoms (VC) (a) and (b) and of boron and nitrogen atoms (VBN) (c) and (d).

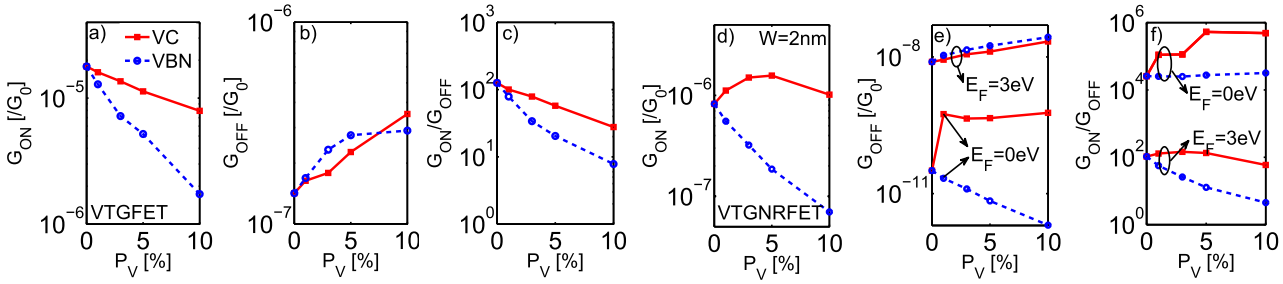

FIG. 10. The dependency of the on-, off-state conductances and on/off conductance ratio on the percentage of vacancies in the cases of VC and VBN for (a)-(c) VTGFET and (d)-(f) VTGNRFET with 6 layers of hBN.

dangling bonds of neighboring nitrogen atoms produce localized states. Density functional theory calculations show that vacancy of boron produces four localized defect states: one at the Fermi level, one around −0.6 eV in the valence band, and two states around 1 eV in the conduction band. The defect state at Fermi level has σ-bonding characteristics and, therefore, it has negligible hybridization with the graphene states with π-bonding characteristics.[30] Due to boron defects, electron transfer takes place from graphene to hBN and the Fermi level decreases.[30] In the case of nitrogen vacancy, however, about one electron is donated from hBN to graphene and the Fermi level increases and graphene becomes n-doped. Nitrogen vacancy results in three localized states: one around Fermi level and two around 1 eV that are nearly degenerate.[30] Furthermore, due to the presence of dangling bonds, a larger DOS of defected hBN in comparison with perfect hBN is observed at energies higher than about 2.5 eV (Refs. 31 and 32) [see the inset of Figs. 8(d) and 9(d)]. This effect results in a higher transmission in defected devices at this energy range and leads to the modest raise of G_{off} in VTGFET and G_{off_1} in VTGNRFET with P_V. At energies lower than 2.5 eV, the transmission probability decreases due to vanishing of hopping between the graphene and hBN layers at some points.

Fig. 10 depicts the on- and off-state conductances and on/off conductance ratio for defected VTGFET and VTGNRFET. As mentioned before, a defected VTGFET exhibits a lower on-state and a larger off-state conductance. In a VTGNRFET in the case of VC, induced midgap states result in a small increase in G_{off_2}. On the other hand, the increase of the bandgap with P_V reduces the transmission in the on-state. Therefore, on-state conductance exhibits a maximum at $P_V = 5\%$. Before the maximum point, the effect of midgap states dominates, whereas at larger vacancy percentages the effect of bandgap increase dominates [see Fig. 9(a)]. In the case of vacancy of boron and nitrogen atoms (VBN), due to uniform suppression of the transmission in the on-state and bandgap energy range, the G_{on} and G_{off_2} decrease as the vacancy percentage increases. On the other hand, because of a larger transmission probability of defected devices in the off-state tunneling region, G_{off} and G_{off_1} increase with P_V [see Figs. 8(c) and 9(c)].

TABLE III. The relative change in the on- and off-state conductances of VTGFET and VTGNRFET with various GNR widths defected by vacancies in the cases of VC and VBN (P = 5%).

W	$\Delta G_{\text{on}}/G_{\text{on}}$(VC)	$\Delta G_{\text{on}}/G_{\text{on}}$(VBN)	$\Delta G_{\text{off}}/G_{\text{off}}$(VC)	$\Delta G_{\text{off}}/G_{\text{off}}$(VBN)
Inf	−0.37	−0.70	0.60	0.94
2	0.91	−0.74	0.68	1.35
3.4	0.40	−0.71	0.64	0.73

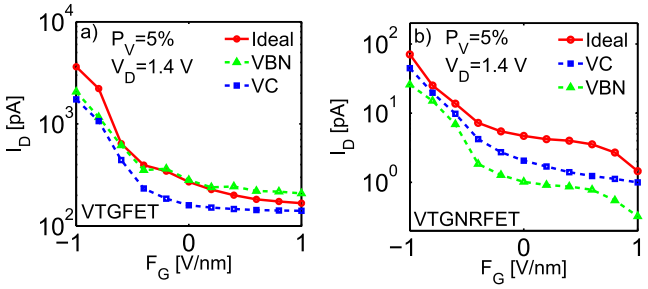

FIG. 11. Drain currents as functions of the applied gate electric field for (a) VTGFET and (b) VTGNRFET in the cases of VC and VBN.

The influence of vacancies on the relative change in the on- and off-state conductances is compared and summarized in Table III. A VTGNRFET with a wider ribbon is only weakly affected by vacancies in comparison with the narrower one. As the ribbon's width increases, the effect of midgap states is less pronounced and the relative change of the conductance decreases.[33] Therefore, VTGFETs are more robust against vacancies compared to VTGNRFETs. The maximum standard deviations of the calculated on/off conductance ratios for 2 nm wide VTGNRFET are 25% and 30.7% for VC and VBN, respectively, and those for VTGFET are 21.5% and 22%.

The effect of introducing vacancy on the transfer characteristics of VTGFET and VTGNRFET in the cases of VC and VBN is depicted in Fig. 11. Defect-enhanced tunneling in the case of VBN defected VTGFETs results in larger tunneling current, especially in the off-state. On the other hand, due to the appearance of midgap states in VC defected VTGNRFETs, the off-current is considerably larger than VBN defected devices. However, due to the increase of the effective bandgap in the presence of VC, the off-current decreases and cannot exceed that of a perfect device.

V. CONCLUSION

We performed a comprehensive statistical analysis to unfold the effect of substrate induced potential fluctuations and vacancies on the characteristics of vertical tunneling FETs based on graphene and GNR heterostructures. To capture atomistic nature of disorder and also quantum transport

in such devices, an atomistic tight-binding band structure model along with the non-equilibrium Green's function formalism are employed. The results indicate that the characteristics of VTGFETs are more robust against disorder compared to VTGNRFETs. In the presence of potential fluctuations, the tunneling current significantly increases, due to increased induced voltage difference between graphene/GNR sheets. In contrast, introducing vacancies reduces the number of available atomic sites and vanishing of hopping between the atomic orbitals and as a consequence reduces the conductance and tunneling current of the VTGFET and VTGNRFET devices. However, introducing vacancies in VTGNRFET can lead to enlargement of energy bandgap and induces midgap states, which increases the transmission probability within the bandgap. The results show that an accurate study of VTGFETs and VTGNRFETs includes a careful consideration of defect-enhanced tunneling.

ACKNOWLEDGMENTS

This work was partly supported by the Iran National Science Foundation.

[1]A. K. Geim and K. S. Novoselov, Nature Mater. **6**, 183 (2007).
[2]L. Ci, L. Song, C. Jin, D. Jariwala, D. Wu, Y. Li, A. Srivastava, Z. F. Wang, K. Storr, L. Balicasa, F. Liu, and P. M. Ajayan, Nature Mater. **9**, 430 (2010).
[3]W. Mehr, J. C. Scheytt, J. Dabrowski, G. Lippert, Y. H. Xie, M. C. Lemme, M. Ostling, and G. Lupina, IEEE Electron Device Lett. **33**, 691 (2012).
[4]L. Britnell, R. V. Gorbachev, R. Jalil, B. D. Belle, F. Schedin, A. Mishchenko, T. Georgiou, M. I. Katsnelson, L. Eaves, S. V. Morozov, N. M. R. Peres, J. Leist, A. K. Geim, K. S. Novoselov, and L. A. Ponomarenko, Science **335**, 947 (2012).
[5]N. Ghobadi and M. Pourfath, IEEE Trans. Electron Devices **61**, 186 (2014).
[6]A. Yazdanpanah, M. Pourfath, M. Fathipour, and H. Kosina, IEEE Trans. Electron Devices **59**, 433 (2012).
[7]A. Y. Goharrizi, M. Pourfath, M. Fathipour, and H. Kosina, IEEE Trans. Electron Devices **59**, 3527 (2012).
[8]N. Djavid, K. Khaliji, S. M. Tabatabaei, and M. Pourfath, IEEE Trans. Electron Devices **61**, 23 (2014).
[9]R. M. Ribeiro and N. M. R. Peres, Phys. Rev. B **83**, 235312 (2011).
[10]J. Sławińska, I. Zasada, and Z. Klusek, Phys. Rev. B **81**, 155433 (2010).
[11]M. P. Anantram, M. S. Lundstrom, and D. E. Nikonov, Proc. IEEE **96**, 1511 (2008).
[12]R. N. Sajjad, C. A. Polanco, and A. W. Ghosh, J. Comput. Electron. **12**, 232 (2013).
[13]T. Low, S. Hong, J. Appenzeller, S. Member, S. Datta, and M. S. Lundstrom, IEEE Trans. Electron Devices **56**, 1292 (2009).
[14]S. B. Kumar, G. Seol, and J. Guo, Appl. Phys. Lett. **101**, 033503 (2012).
[15]C. H. Lewenkopf, E. R. Mucciolo, and A. H. C. Neto, Phys. Rev. B **77**, 081410 (2008).
[16]J. Martin, N. Akerman, G. Ulbricht, T. Lohmann, J. H. Smet, K. von Klitzing, and A. Yacoby, Nat. Phys. **4**, 144 (2008).
[17]C. Stampfer, J. Gttinger, S. Hellmller, F. Molitor, K. Ensslin, and T. Ihn, Phys. Rev. Lett. **102**, 056403 (2009).
[18]M. Poljak, S. Member, E. B. Song, M. Wang, T. Suligoj, and K. L. Wang, IEEE Trans. Electron Devices **59**, 3231 (2012).
[19]Y. Y. Illarionov, A. Smith, S. Vaziri, M. Ostling, T. Mueller, M. Lemme, and T. Grasser, Appl. Phys. Lett. **105**, 143507 (2014).
[20]W. Wang, V. Reddy, and A. T. Krishnan, IEEE Trans. Device Mater. Reliab. **7**, 509 (2007).
[21]A. Asenov, A. R. Brown, J. H. Davies, S. Kaya, and G. Slavcheva, IEEE Trans. Electron Devices **50**, 1837 (2003).
[22]V. J. Surya, K. Iyakutti, H. Mizuseki, and Y. Kawazoe, IEEE Trans. Nanotechnol. **11**, 534 (2012).
[23]V. M. Pereira, J. M. B. L. dos Santos, and A. H. C. Neto, Phys. Rev. B **77**, 115109 (2008).
[24]S. Chang, Y. Zhang, Q. Huang, H. Wang, and G. Wang, Micro Nano Lett. **8**, 816 (2013).
[25]M. Y. Han, J. C. Brant, and P. Kim, Phys. Rev. Lett. **104**, 056801 (2010).
[26]L. Song, L. Ci, H. Lu, P. B. Sorokin, C. Jin, J. Ni, A. G. Kvashnin, D. G. Kvashnin, J. Lou, B. I. Yakobson, and P. M. Ajayan, Nano Lett. **10**, 3209 (2010).
[27]A. Zobelli, C. P. Ewels, A. Gloter, G. Seifert, O. Stephan, S. Csillag, and C. Colliex, Nano Lett. **6**, 1955 (2006).
[28]Z. L. Hou, M. S. Cao, J. Yuan, X. Y. Fang, and X. L. Shi, J. Appl. Phys. **105**, 076103 (2009).
[29]W. Orellana and H. Chacham, Phys. Rev. B **63**, 125205 (2001).
[30]S. Park, C. Park, and G. Kim, J. Chem. Phys. **140**, 134706 (2014).
[31]M. S. Si and D. S. Xue, Phys. Rev. B **75**, 193409 (2007).
[32]S. Azevedo, J. R. Kaschny, C. M. C. de Castilho, and F. de Brito Mota, Eur. Phys. J. B **67**, 507 (2009).
[33]E. R. Mucciolo, A. H. C. Neto, and C. H. Lewenkopf, Phys. Rev. B **79**, 075407 (2009).